

# An efficient method to prepare high-performance dye-sensitized photoelectrodes using ordered TiO<sub>2</sub> nanotube arrays and TiO<sub>2</sub> quantum dot blocking layers

Zhang Lan<sup>1,2,3</sup> · Wanxia Wu<sup>1,2,3</sup> · Sheng Zhang<sup>1,2,3</sup> · Lanfang Que<sup>1,2,3</sup> · Jihuai Wu<sup>1,2,3</sup>

Received: 22 February 2016 / Revised: 23 May 2016 / Accepted: 26 May 2016 / Published online: 2 June 2016  
© Springer-Verlag Berlin Heidelberg 2016

**Abstract** High-performance dye-sensitized photoelectrodes using ordered TiO<sub>2</sub> nanotube arrays (TNTs) and TiO<sub>2</sub> quantum dot blocking layers are fabricated. The free-standing TNT membranes with perfect ordered morphology are prepared by three times of anodic oxidation on Ti foils. These TNT membranes can be easily transported to conductive glasses to fabricate front-side illuminated photoelectrodes. By changing anodic oxidation duration, the thickness of TNT membranes can be controlled, which shows significant influence on the UV-Vis reflectance and absorption abilities of TNT-based photoelectrodes and further influence photovoltaic performance of dye-sensitized solar cells (DSSCs). The highest power conversion efficiency (*PCE*) of DSSCs about 6.21 % can be obtained by using TNT membranes prepared with anodic oxidation of 3 h. For further improving photovoltaic performance of DSSCs, TiO<sub>2</sub> quantum dot (QDs) blocking layers are inserted between conductive glasses and TNT membranes in the photoelectrodes, which show remarkable effects. The highest *PCE* of DSSCs with this kind of blocking layers can increase to 8.43 %, producing 35.75 % enhancement compared with that of the counterparts without TiO<sub>2</sub> QD blocking layers.

**Keywords** TiO<sub>2</sub> nanotube array · TiO<sub>2</sub> quantum dot · Blocking layer · Photoelectrode

## Introduction

Dye-sensitized solar cells (DSSCs) have been intensively studied in the past decades owing to their outstanding characteristics such as low cost, high power conversion efficiency (*PCE*), and easy preparation [1, 2]. As an important component of DSSCs, the photoelectrode is usually prepared with wide-band-gap semiconductor nanocrystal oxides including TiO<sub>2</sub>, SnO<sub>2</sub>, and ZnO [3–5]. These nanocrystal oxides have large surface area, which can adsorb sufficient dyes for efficient utilization of sunlight. However, the transportation of photogenerated electrons in the nanocrystal oxide films is trap limited, and the photogenerated electrons need to diffuse through 10<sup>3</sup>–10<sup>6</sup> nanoparticles to reach the conductive substrate [6, 7]. So, the existed tremendous crystalline boundaries and disordered pore structures in the nanocrystal oxide films can cause serious dark reaction, which affects photovoltaic performance of DSSCs.

Highly ordered TiO<sub>2</sub> nanotube arrays by anodic oxidation of Ti foils have attracted many attentions and been intensively investigated as substitutes for mesoporous nanoparticle films in DSSCs [8–11]. TiO<sub>2</sub> nanotube arrays (NTs) have some distinct characteristics suitable for preparing highly photovoltaic performance of DSSCs [12–14]. Firstly, TiO<sub>2</sub> NTs are able to provide big surface area result in large dye-loading amount for efficient absorption of sun light; secondly, the ordered walls of TiO<sub>2</sub> nanotubes can give superior electron transport channels, which can enhance electron transport rate and decrease dark reaction; thirdly, the ordered 50–100-nm size of pores in the TiO<sub>2</sub> NTs benefit for deep penetration of liquid electrolyte and formation of good interfacial contacts.

✉ Zhang Lan  
lanzhang@hqu.edu.cn

<sup>1</sup> Engineering Research Center of Environment-Friendly Functional Materials, Ministry of Education, Huaqiao University, Xiamen 361021, China

<sup>2</sup> Key Laboratory of Functional Materials for Fujian Higher Education, Huaqiao University, Xiamen 361021, China

<sup>3</sup> Institute of Materials Physical Chemistry, Huaqiao University, Xiamen 361021, China

At the same time, the ordered TiO<sub>2</sub> NTs, metal oxide-TiO<sub>2</sub> composite NTs, and the doped ones are good photocatalysts for dye degradation or water splitting. M. M. Momeni's group has done a systematic research in the field. They use very simple methods to prepare Ta<sub>2</sub>O<sub>5</sub> NTs and nanowires [15, 16], Cr-doped TiO<sub>2</sub> NTs [17, 18], Mn-doped TiO<sub>2</sub> NTs [19], Fe-doped TiO<sub>2</sub> NTs [20], Cu-doped TiO<sub>2</sub> NTs [21], ZnO-TiO<sub>2</sub> composite NTs [22, 23], WO<sub>3</sub>-TiO<sub>2</sub> composite NTs [24], Co-doped WO<sub>3</sub>-TiO<sub>2</sub> composite NTs [25, 26], Cu-doped WO<sub>3</sub>-TiO<sub>2</sub> composite NTs [27], Pt/WO<sub>3</sub>-TiO<sub>2</sub> composite NTs [28], Au/WO<sub>3</sub>-TiO<sub>2</sub> composite NTs [29], and PbO/WO<sub>3</sub>-TiO<sub>2</sub> composite NTs [30]. These materials show highly photocatalytic activity in degrading dyes or splitting water.

Here, we report the fabricating details of highly ordered TiO<sub>2</sub> NTs and their application in front-side illuminated photoelectrodes. In order to enhance photovoltaic performance of DSSCs, TiO<sub>2</sub> QD blocking layers are inserted into TiO<sub>2</sub> NT-based photoelectrodes. It has been demonstrated that TiO<sub>2</sub> QD blocking layers can effectively suppress dark reaction in photoelectrodes of DSSCs [31], so taking into accounts of the merits of TiO<sub>2</sub> NTs and special function of TiO<sub>2</sub> QD blocking layers for DSSCs, the preparation of high-efficiency DSSCs can be expected.

## Experimental section

### Materials

All reagents including 2-propanol, ethanol, ethylene glycol, ammonium fluoride, hydrogen peroxide aqueous solution (30 wt.%), tetra-*n*-butyl titanate, chloroplatinic acid hexahydrate, acetic acid, acetonitrile, titanium tetrachloride, tetra-butyl ammonium iodide, 4-*tert*-butyl pyridine, sodium iodide, and iodine were analytical reagent grade, purchased from Aladdin Chemical Reagent Co., Ltd., and used without further treatment. Ti foils (0.2 mm thick, 99 wt.% purity) were purchased from Bao Ji Yun Jie Metal Production Co., Ltd. Conductive glasses (FTO glass, fluorine-doped tin oxide over-layer, sheet resistance 15 Ω square<sup>-1</sup>) were purchased from Nippon Sheet Glass Co. JP. N719 dye (Ru [LL'-(NCS)<sub>2</sub>], L = 2, 2'-bipyridyl-4,4'-dicarboxylic acid, L' = 2, 2'-bipyridyl-4,4'-ditetrabutylammonium carboxylate) was purchased from Dyesol.

### Preparation of free-standing TiO<sub>2</sub> nanotube array membranes

The preparation of TiO<sub>2</sub> nanotube arrays includes the following steps [32]. Firstly, Ti foils (2 × 3 cm) were treated with ultrasonic cleanser in deionized water, 2-propanol, and ethanol for 5 min, respectively, and then rinsed with ethanol and dried at room temperature. Secondly, the cleaned Ti foils were

subjected to anodic oxidation at room temperature at 50 V for 1 h. The electrolytic cell composes two cleaned Ti foils as electrodes and an electrolyte containing ethylene glycol, H<sub>2</sub>O, and ammonium fluoride with weight ratio of 98:2:0.3. Thirdly, the formed TiO<sub>2</sub> nanotube array membranes on Ti foils (marked as TNT-1<sup>th</sup>s) were peeled off with ultrasonic treatment in deionized water. Then, the Ti foils were anodized again at 50 V for 1 to 5 h in the same electric cell with the same electrolyte. Fourthly, the obtained TiO<sub>2</sub> nanotube array membranes on Ti foils (marked as TNT-2<sup>th</sup>s) were sintered at 450 °C for 2 h. After cooled down to room temperature, the Ti foils with sintered TNT-2<sup>th</sup>s were anodized for the third time at 80 V for 5 min in the same condition (marked as TNT-3<sup>th</sup>). Then, the Ti foils were dipped into 30 wt.% H<sub>2</sub>O<sub>2</sub> aqueous solution for 1 h to strip sintered TNT-2<sup>th</sup>s away from Ti foils. Thus far, the free-standing TNT-2<sup>th</sup>s are obtained.

### Preparation of TiO<sub>2</sub> nanotube array-based photoelectrodes

The TiO<sub>2</sub> nanotube array-based photoelectrodes without TiO<sub>2</sub> QD blocking films were fabricated by transferring TNT-2<sup>th</sup>s to FTO glasses, and then, the membranes were clung on FTO glasses with 20-nm TiO<sub>2</sub> nanoparticles as cementing agent and thermally treated at 450 °C for 30 min [12].

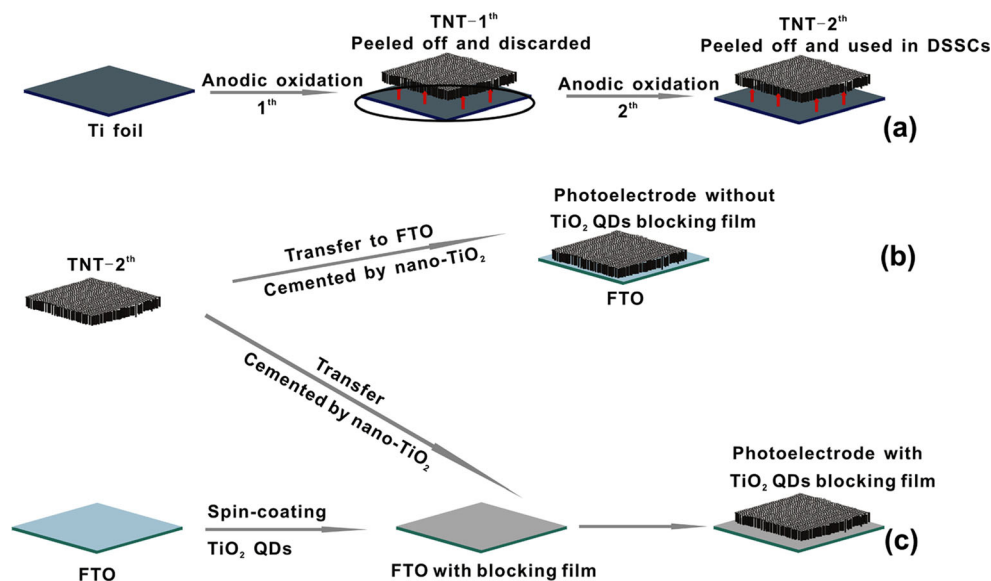
The TiO<sub>2</sub> nanotube array-based photoelectrodes with TiO<sub>2</sub> QD blocking films were prepared as follows. Firstly, TiO<sub>2</sub> QD toluene solution (average size about 3.6 nm and concentration about 0.07 g ml<sup>-1</sup>) were spin coated on FTO glasses and then sintered at 450 °C for 30 min according to the reference [31]. Later, the TNT-2<sup>th</sup>s were clung on TiO<sub>2</sub> QD blocking films with the same method as that of the membranes being cemented on FTO glasses directly.

The as-prepared photoelectrodes were treated with 0.05 M TiCl<sub>4</sub> aqueous solution at 70 °C for 30 min, later sintered again at 450 °C for 30 min. After cooled down to room temperature, the photoelectrodes were dipped into 0.25 M N719 alcohol solution for 24 h to form dye-sensitized photoelectrodes. For better understanding, the schematic diagram of preparing free-standing TNT-2<sup>th</sup>s and photoelectrodes without and with TiO<sub>2</sub> QD blocking films is shown in Scheme 1.

### Assembling of dye-sensitized solar cells

A photoelectrode and a platinum counter electrode were clipped together. One drop of liquid electrolyte was kept between the two electrodes. A piece of cyano acrylate adhesive (30 μm) was used as sealant. Bisphenol A epoxy resin was used for further sealing process. The liquid electrolyte contained 0.4 M sodium iodide, 0.1 M tetrabutyl ammonium iodide, 0.5 M 4-*tert*-butylpyridine, and 0.05 M iodine of acetonitrile solution.

**Scheme 1** Schematic diagram of preparing free-standing TNT-2<sup>th</sup>s (a) and photoelectrodes without (b)/with (c) TiO<sub>2</sub> QD blocking films



## Measurements

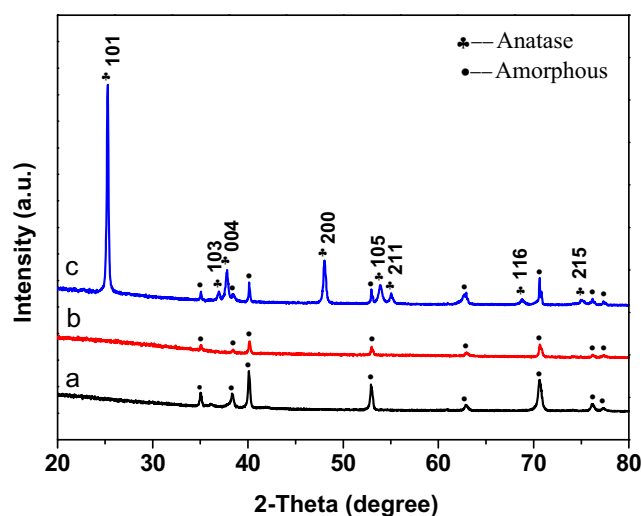
The morphologies of TiO<sub>2</sub> nanotube arrays were observed by a field emission scanning electron microscopy (FESEM; S-4800, Hitachi) and a field emission transmission electron microscopy (FETEM; JEM-2100). X-ray diffraction (XRD) measurements were carried out with a Bruker D8, using Cu K<sub>α1</sub> radiation ( $\lambda$ ; 0.154059 nm). UV-Vis absorption spectra were measured with a UV-Vis 3100 spectrophotometer (Shimadzu, Japan). Photovoltaic performance tests [photocurrent density-voltage ( $J$ - $V$ ) curves] were carried out with PVIV-94043A system (AM 1.5 G, 100 mW cm<sup>-2</sup> from no. 94043A solar simulator, Newport, USA) in ambient atmosphere and recorded with a Keithly 2400 source meter. Incident photo-current conversion efficiency ( $IPCE$ ) curves were measured as a function of wavelength from 300 to 800 nm using a Newport IPCE system (Newport, USA). All of DSSCs were measured five times and the average data were taken. The active area of DSSCs was 0.12 cm<sup>2</sup> (0.3 × 0.4 cm<sup>2</sup>).

## Results and discussion

Figure 1 shows XRD patterns of (a) Ti foil, (b) TiO<sub>2</sub> nanotube arrays without thermal treatment, and (c) TiO<sub>2</sub> nanotube arrays with thermal treatment at 450 °C for 2 h. One can observe that the XRD pattern of TiO<sub>2</sub> nanotube arrays without thermal treatment is the same as that of Ti foil, which is consistent with the standard PDF (JCPDS nos. 44–1294) of Ti metal, so the formed TiO<sub>2</sub> nanotube arrays is amorphous. Whereas, after thermal treatment at 450 °C for 2 h, the specific diffraction peaks at 25.3°, 36.9°, 37.8°, 48.0°, 53.9°, 55.1°, 68.8°, and 75.0° appear, which correspond to (101), (103), (004), (200), (105), (211), (116), and (215) of crystal planes of anatase TiO<sub>2</sub>

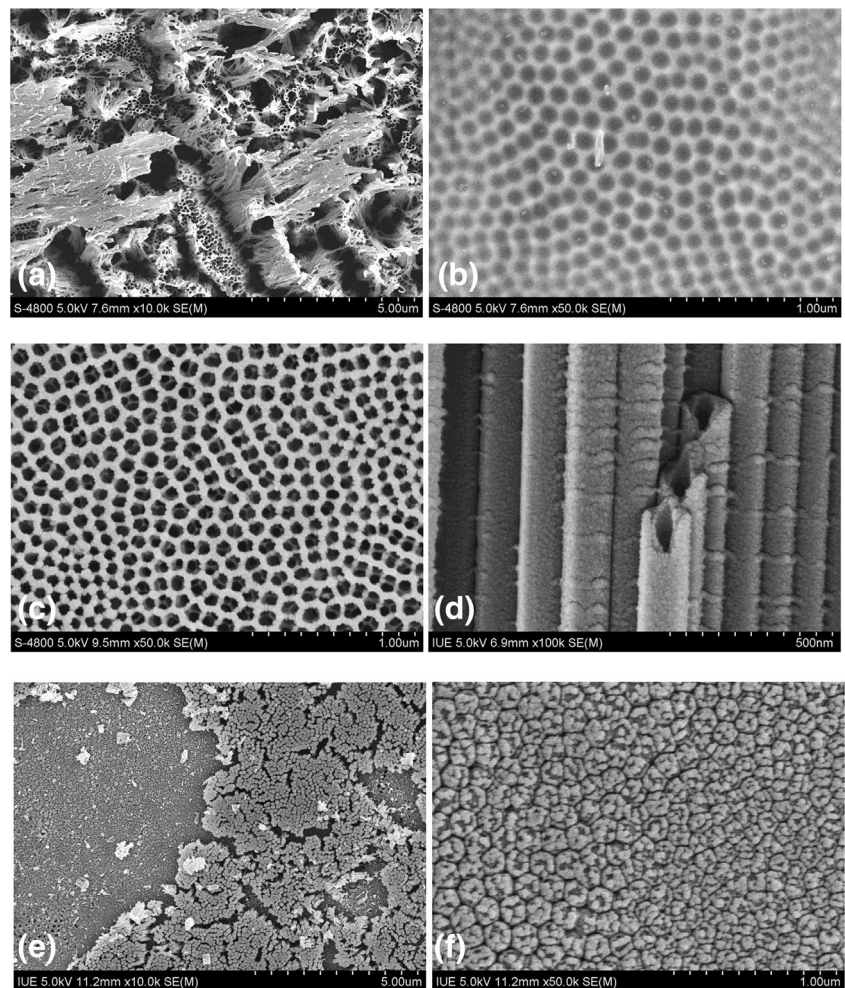
(JCPDS no. 21–1272) [33]. No other impurity peaks are observed. Therefore, it can be concluded that after thermal treatment, the amorphous TiO<sub>2</sub> nanotube arrays can be turned into anatase crystalline TiO<sub>2</sub> nanotube arrays.

Figure 2 shows the morphologies of TNT-1<sup>th</sup> (a), Ti foil after being peeled off TNT-1<sup>th</sup> (b), TNT-2<sup>th</sup> (c), cross-sectional view of TNT-2<sup>th</sup> (d), and bottom-side views of free-standing TNT-2<sup>th</sup> after being stripped away from Ti foil (e and f). It can be seen that the structure of TNT-1<sup>th</sup> has some defects including big cracks, large cavities, and some nanowire bundles on the surface. After the TNT-1<sup>th</sup> being peeled off, highly ordered bottom structure appears on the Ti foil. The second time of anodic oxidation is occurred on the ordered bottom structure on the Ti foil. Thanks to the guide of this ordered bottom structure, highly ordered TNT-2<sup>th</sup> is obtained as shown in Fig. 2c, d. The third time of anodic oxidation is carried out



**Fig. 1** XRD patterns of a Ti foil, b TiO<sub>2</sub> nanotube arrays without thermal treatment, and c TiO<sub>2</sub> nanotube arrays with thermal treatment at 450 °C for 2 h

**Fig. 2** SEM images of **a** TNT-1<sup>th</sup>, **b** Ti foil after being peeled off TNT-1<sup>th</sup>, **c** TNT-2<sup>th</sup>, **d** cross-sectional view of TNT-2<sup>th</sup>, and **e**, **f** bottom-side view of free-standing TNT-2<sup>th</sup> after being stripped away from Ti foil



to form an amorphous TNT-3<sup>th</sup> under the sintered TNT-2<sup>th</sup>. Because the amorphous TNT-3<sup>th</sup> can be easily dissolved by 30 wt.% H<sub>2</sub>O<sub>2</sub> aqueous solution, nevertheless, the sintered anatase crystalline TNT-2<sup>th</sup> is hard to be dissolved [32], so the free-standing TNT-2<sup>th</sup> can be obtained after 30 wt.% H<sub>2</sub>O<sub>2</sub> aqueous solution treatment. As presented in Fig. 2e, f, part of dissolved thin layer of TNT-3<sup>th</sup> can be clearly seen, and some holes appear on the dissolved places of TNT-3<sup>th</sup>, which verifies the formation of double-side opened TNT-2<sup>th</sup>.

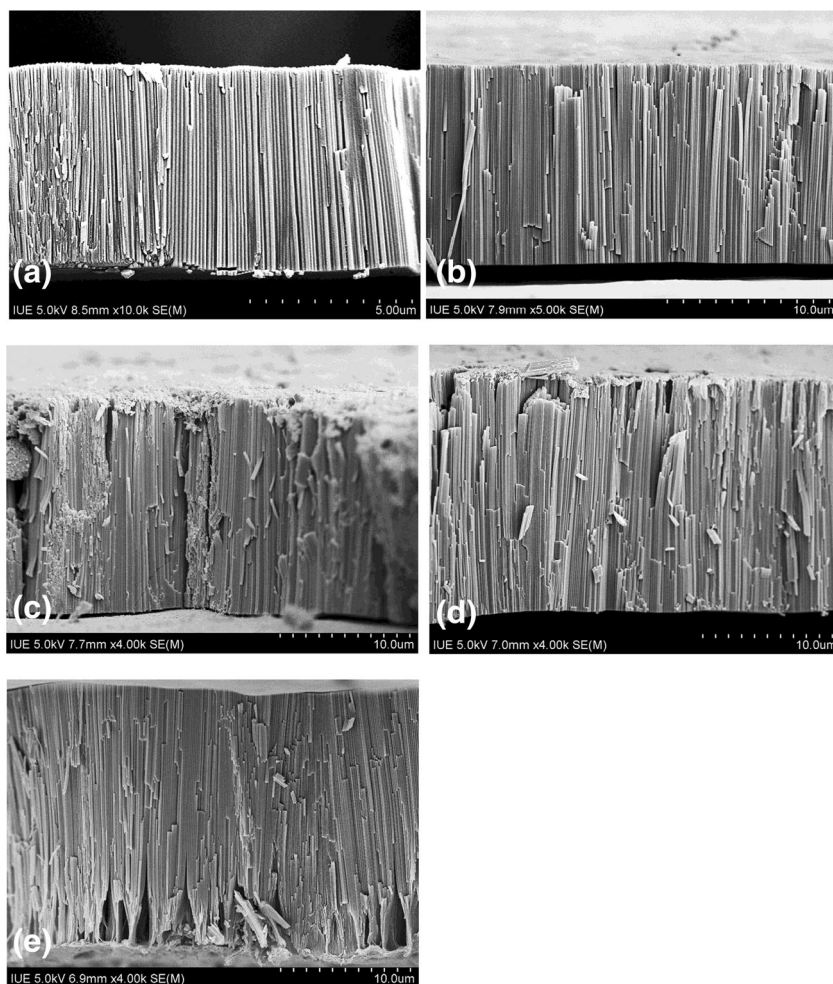
Figure 3 is the cross-sectional SEM images of TNT-2<sup>th</sup>s prepared with different anodic oxidation duration from 1 to 5 h. All of the samples have ordered structure, and their thicknesses are 6.2, 12.2, 16.7, 18.4, and 19.6 μm, respectively. From the changed thickness of these samples, we can find that the growth rate of TNT-2<sup>th</sup>s decreases by going with the extended reaction time, which is owing to the gradually consumed ammonium fluoride and its decreased concentration in the electrolyte.

In order to investigate the structure information details of TNT-2<sup>th</sup>, TEM, high-resolution TEM (HRTEM), and selected area electron diffraction (SAED) images are measured and

shown in Fig. 4. From Fig. 4a, one can find that the inside and outside diameters of TNT-2<sup>th</sup> are 60 and 100 nm, respectively, and the thickness of the tube wall is about 20 nm. In HRTEM image (Fig. 4b), the distance between two adjacent planes is measured to be 0.477 and 0.374 nm, corresponding to the (001) and (100) planes in the anatase phase of TiO<sub>2</sub> [34]. From the image of SAED as shown in Fig. 4c, it can be concluded that the synthesized TiO<sub>2</sub> nanotubes with thermal treatment are highly crystalline anatase polycrystal [35].

Figure 5 shows the UV-Vis diffuse reflectance spectra of TNT-2<sup>th</sup>-based photoelectrodes (a) and absorption spectra of dye-sensitized TNT-2<sup>th</sup>-based photoelectrodes (b). From Fig. 5a, one can see that in the short wavelength range of 300 to 400 nm, the diffuse reflectance data of TNT-2<sup>th</sup>-based photoelectrodes are small, owing to the strong absorption coefficient of TiO<sub>2</sub> nanomaterials in this wavelength range [36]. By going with the increased wavelength, the diffuse reflectance data increase gradually, and the highest ones appear in the wavelength range of 550 to 650 nm. Furthermore, the diffuse reflectance ability of TNT-2<sup>th</sup>-based photoelectrodes in the wavelength range of 500 to 800 nm is increased with

**Fig. 3** Cross-sectional SEM images of TNT-2<sup>th</sup>s prepared with different anodic oxidation duration, **a** 1, **b** 2, **c** 3, **d** 4, and **e** 5 h



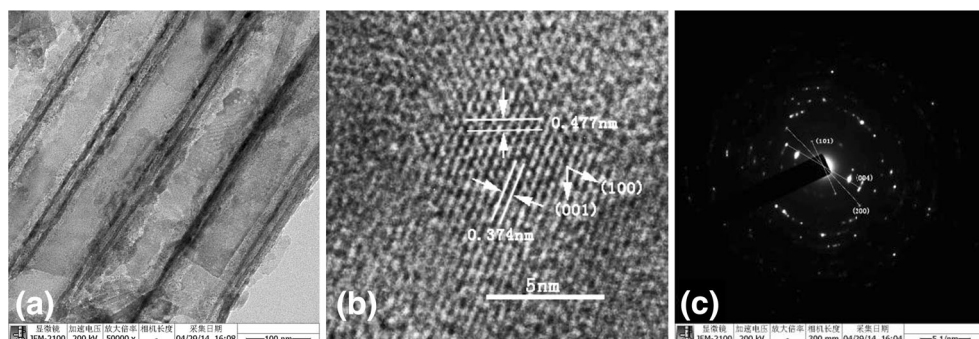
the extended time of anodic oxidation, which is mainly due to the increased thickness of TNT-2<sup>th</sup> as shown in Fig. 3.

Figure 5b is the UV-Vis absorption spectra of dye-sensitized TNT-2<sup>th</sup>-based photoelectrodes. The absorbance of dye-sensitized TNT-2<sup>th</sup>-based photoelectrodes is strong in the wavelength range of 300 to 570 nm and then becomes weak in high wavelength range of 570 to 800 nm. The absorbance of dye-sensitized TNT-2<sup>th</sup>-based photoelectrodes in the UV wavelength region is mainly induced by the intrinsic character of TiO<sub>2</sub> nanomaterials. In the Vis-NIR wavelength region, the changed absorbance of dye-sensitized TNT-2<sup>th</sup>-

based photoelectrodes is caused by the absorbance character of sensitized N719 dye, which has strong absorbance in wavelength region of 400 to 570 nm and weak absorbance in the longer wavelength [37]. Along with the increased thickness of TNT-2<sup>th</sup>, the absorbance of dye-sensitized TNT-2<sup>th</sup>-based photoelectrodes is also increased in the main wavelength region of 400 to 570 nm because of the increased adsorbed amounts of dyes on the longer TNT-2<sup>th</sup>.

Figure 6 presents the *J-V* curves of DSSCs with TNT-2<sup>th</sup>-based photoelectrodes with and without TiO<sub>2</sub> QD blocking layers. The main photovoltaic parameters including open-

**Fig. 4** TEM (a), HRTEM (b), and SAED (c) images of TNT-2<sup>th</sup>



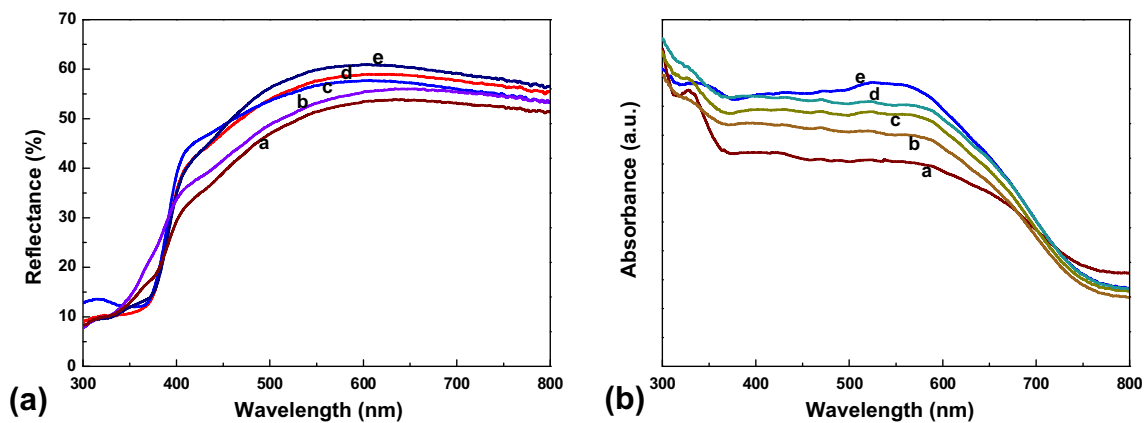


**Fig. 5** UV-Vis diffuse reflectance spectra of TNT-2<sup>th</sup>-based photoelectrodes (a) and absorption spectra of dye-sensitized TNT-2<sup>th</sup>-based photoelectrodes (b). The letters of *a*, *b*, *c*, *d*, and *e* correspond to the anodic oxidation durations of 1, 2, 3, 4, and 5 h, respectively

circuit voltage ( $V_{OC}$ ), short-circuit current density ( $J_{SC}$ ), fill factor ( $FF$ ), and  $PCE$  are summarized in Table 1. For the DSSCs without  $TiO_2$  QD blocking layers, the values of  $V_{OC}$  change little. It is known that  $V_{OC}$  is mainly determined by the difference of Fermi level of semiconductor in the photoelectrode and redox potential of iodide/iodine ions in the electrolyte [38]. These five cells have similar structure and use the same electrolyte, and the changed thickness of TNT-2<sup>th</sup>s has little influence on the value of Fermi level [39], so the  $V_{OC}$  change little. The same case exists in the DSSCs with  $TiO_2$  QD blocking layers, so these cells also have similar  $V_{OC}$ . Comparing the two kinds of DSSCs, it is found that the DSSCs with  $TiO_2$  QD blocking layers have higher  $V_{OC}$  than that of the DSSCs without  $TiO_2$  QD blocking layers, which is owing to the effect of  $TiO_2$  QD blocking layers of reducing dark reaction in the DSSCs.

From Table 1, we can see that the change tendencies of  $J_{SC}$  of the DSSCs without and with  $TiO_2$  QD blocking layers are similar. Namely, they all increase to maximum values with the increased thickness of TNT-2<sup>th</sup> by extending anodic oxidation duration to 3 h and then decrease with longer anodic oxidation time. The UV-Vis diffuse reflectance and absorption spectra of

these photoelectrodes shown in Fig. 5 reveal that the diffuse reflectance ability of TNT-2<sup>th</sup>-based photoelectrodes and the absorption strength of dye-sensitized TNT-2<sup>th</sup>-based photoelectrodes are both improved by going with the extended anodic oxidation duration, which favor efficient utilization of incident light. However, with the increased length of electronic transporting channels in thicker TNT-2<sup>th</sup>, the recombination reactions also increase at the same time [40]. So, the two opposite influences will result in a balance point, at which the  $J_{SC}$  will attain to a maximum value.

The IPCE data are shown in Fig. 7 for better illustrating the changed values of  $J_{SC}$ . From Fig. 7, we can see that the IPCE of DSSCs increases firstly and then decreased by going with the extended anodic oxidation duration, and the highest value is achieved when the TNT-2<sup>th</sup> was prepared by 3-h anodic oxidation. This tendency is accordance with that of  $J_{SC}$ . However, it should be point out that in the long wavelength (>650 nm), the IPCE of DSSCs has a little different variation trend as that of aforementioned and is also different with that of UV-Vis diffuse reflectance and absorption spectra. The reason is mainly owing to the dark recombination effect in the DSSCs with thicker TNT-2<sup>th</sup>. Nevertheless, the DSSCs with

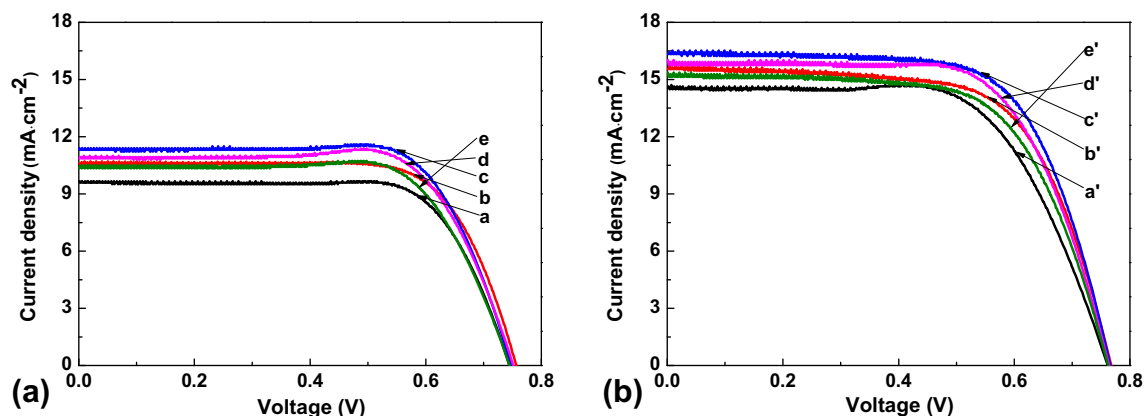


**Fig. 6**  $J$ - $V$  curves of DSSCs with TNT-2<sup>th</sup>-based photoelectrodes. The letters of *a*, *b*, *c*, *d*, and *e* and *a'*, *b'*, *c'*, *d'*, and *e'* correspond to DSSCs without and with  $TiO_2$  QD blocking layers, respectively. The letters of *a*-*a'*, *b*-*b'*, *c*-*c'*, *d*-*d'*, and *e*-*e'* represent different anodic oxidation duration as illustrated in Fig. 5

**Table 1** Photovoltaic parameters of DSSCs presented in Fig. 6

Photoelectrode	$V_{OC}$ (V)	$J_{SC}$ (mA cm <sup>-2</sup> )	$FF$	$PCE$ (%)
<i>a</i>	0.744	9.66	0.730	5.25
<i>b</i>	0.756	10.59	0.726	5.81
<i>c</i>	0.748	11.44	0.726	6.21
<i>d</i>	0.751	10.85	0.739	6.02
<i>e</i>	0.745	10.36	0.730	5.63
<i>a'</i>	0.761	14.56	0.651	7.21
<i>b'</i>	0.767	15.52	0.660	7.85
<i>c'</i>	0.766	16.28	0.676	8.43
<i>d'</i>	0.764	15.99	0.667	8.15
<i>e'</i>	0.762	15.36	0.644	7.54

higher reflectance of TNT-2<sup>th</sup>, such as samples of *c'*, *d'*, and *e'*, still show higher IPCE in long wavelength than that of the samples of *a'* and *b'*.

From the data, it is clearly seen that all of the five DSSCs with TiO<sub>2</sub> QD blocking layers have higher  $J_{SC}$  than that of the DSSCs without TiO<sub>2</sub> QD blocking layers, owing to the effective reduced dark reaction in the former cells by the TiO<sub>2</sub> QD blocking layers. It also can be found that all of the DSSCs with TiO<sub>2</sub> QD blocking layers have lower  $FF$  than that of the counterparts without TiO<sub>2</sub> QD blocking layers. The reason is that the addition of TiO<sub>2</sub> QD blocking layers would also increase the intrinsic resistance of the cells, which results in the decreased  $FF$  [41].

The combined results of the changed values of  $V_{OC}$ ,  $J_{SC}$ , and  $FF$  bring to the changed  $PCE$ . And, the highest  $PCE$  of DSSCs without and with TiO<sub>2</sub> QD blocking layers can attain to 6.21 and 8.43 %, respectively. Therefore, the utilization of TiO<sub>2</sub> QD blocking layers is an efficient way to enhance photovoltaic performance of TNT-based DSSCs.

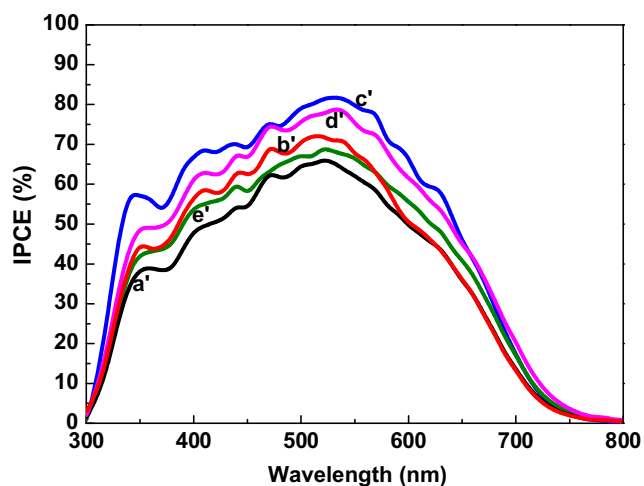


**Fig. 7** IPCE curves of DSSCs with TNT-2<sup>th</sup>-based photoelectrodes. The letters of *a'*, *b'*, *c'*, *d'*, and *e'* correspond to the anodic oxidation duration of 1, 2, 3, 4, and 5 h, respectively

## Conclusions

Using three times of anodic oxidation on Ti foils combining with thermal treatment, high-crystalline polycrystal free-standing TNT membranes with perfectly ordered morphology are fabricated. The thickness of TNT membranes can be well controlled by changing anodic oxidation duration. When they are transported to conductive glasses to fabricate front-side illuminated photoelectrodes, the thickness of TNT membranes has significant influences on the UV-Vis reflectance and absorption abilities of TNT-based photoelectrodes and further influence photovoltaic performance of DSSCs. It is found that the DSSCs with TNT-based photoelectrodes by anodic oxidation of 3 h can attain to the highest  $PCE$  about 6.21 %. For further improving photovoltaic performance of DSSCs, TiO<sub>2</sub> QD blocking layers are used to reduce dark reaction, which bring about improved  $V_{OC}$ ,  $J_{SC}$ , and finally the enhanced  $PCE$ . It is shown that by utilizing TiO<sub>2</sub> QD blocking layers, the best performance of DSSCs has  $PCE$  about 8.43 %, with 35.75 % enhancement compared with that of the counterparts without TiO<sub>2</sub> QD blocking layers, so it is an efficient way to improve photovoltaic performance of DSSCs with TNT-based photoelectrodes.

**Acknowledgments** The authors would like to acknowledge the supports of the National Natural Science Foundation of China (Nos. U1205112, 51002053, and 61474047), the Fujian Provincial Science Foundation for Distinguished Young Scholars (2015J06011), the Programs for Prominent Young Talents and New Century Excellent Talents in Fujian Province University, and the Promotion Program for Young and Middle-aged Teacher in Science and Technology Research of Huaqiao University (ZQN-YX102).

## References

1. Wu J, Lan Z, Lin J, Huang M, Huang Y, Fan L, Luo G (2015) Electrolytes in dye-sensitized solar cells. *Chem Rev* 115:2136–2173
2. Bella F, Gerbaldi C, Barolo C, Grätzel M (2015) Aqueous dye-sensitized solar cells. *Chem Soc Rev* 44:3431–3473
3. Lan Z, Wu J, Lin J, Huang M (2014) TiCl<sub>4</sub> assisted formation of nano-TiO<sub>2</sub> secondary structure in photoactive electrodes for high efficiency dye-sensitized solar cells. *Sci China Chem* 57:888–894
4. Lan Z, Liu L, Huang M, Wu J, Lin J (2015) Preparation of nano-flower-like SnO<sub>2</sub> particles and their applications in efficient CdS quantum dots sensitized solar cells. *J Mater Sci Mater Electron* 26: 7914–7920
5. Szkoda M, Siuzdak K, Oleksiak AL (2016) Optimization of electrochemical doping approach resulting in highly photoactive iodine-doped titania nanotubes. *J Solid State Electrochem* 20: 563–569
6. Benkstein KD, Kopidakis N, Lagemaat JVD, Frank AJ (2003) Influence of the percolation network geometry on electron transport in dye-sensitized titanium dioxide solar cells. *J Phys Chem B* 107: 7759–7767
7. Lagemaat JVD, Frank AJ (2001) Nonthermalized electron transport in dye-sensitized nanocrystalline TiO<sub>2</sub> films: transient photocurrent

- and random-walk modeling studies. *J Phys Chem B* 105:11194–11205
8. Ananthakumar S, Ramkumar J, Babu SM (2014) Effect of co-sensitization of CdSe nanoparticles with N3 dye on TiO<sub>2</sub> nanotubes. *Sol Energy* 106:136–142
  9. Kuang D, Brillet J, Chen P, Takata M, Uchida S, Miura H, Sumioka K, Zakeeruddin SM, Grätzel M (2008) Application of highly ordered TiO<sub>2</sub> nanotube arrays in flexible dye-sensitized solar cells. *ACS Nano* 2:1113–1116
  10. Qi L, Yin Z, Zhang S, Ouyang Q, Li C, Chen Y (2014) The increased interface charge transfer in dye-sensitized solar cells based on well-ordered TiO<sub>2</sub> nanotube arrays with different lengths. *J Mater Res* 29:745–752
  11. Momeni MM, Hosseini MG (2015) Different TiO<sub>2</sub> nanotubes for back illuminated dye sensitized solar cell: fabrication, characterization and electrochemical impedance properties of DSSCs. *J Mater Sci Mater Electron* 25:5027–5034
  12. Gao S, Lan Z, Wu W, Que L, Wu J, Lin J, Huang M (2014) Fabrication and photovoltaic performance of high efficiency front-illuminated dye-sensitized solar cell based on ordered TiO<sub>2</sub> nanotube arrays. *Acta Phys -Chim Sin* 30:446–452
  13. Jennings JR, Ghicov A, Peter LM, Schmuki P, Walker AB (2008) Dye-sensitized solar cells based on oriented TiO<sub>2</sub> nanotube arrays: transport, trapping, and transfer of electrons. *J Am Chem Soc* 130:13364–13372
  14. Zeng T, Ni H, Su X, Chen Y, Jiang Y (2015) Highly crystalline titania nanotube arrays realized by hydrothermal vapor route and used as front-illuminated photoanode in dye sensitized solar cells. *J Power Sources* 283:443–451
  15. Momeni MM, Mirhosseini M, Chavoshi M, Hakimzade A (2016) The effect of anodizing voltage on morphology and photocatalytic activity of tantalum oxide nanostructure. *J Mater Sci Mater Electron* 27:3941–3947
  16. Momeni MM, Mirhosseini M, Chavoshi M (2016) Growth and characterization of Ta<sub>2</sub>O<sub>5</sub> nanorod and WTa<sub>2</sub>O<sub>5</sub> nanowire films on the tantalum substrates by a facile one-step hydrothermal method. *Ceram Int* 42:9133–9138
  17. Momeni MM, Ghayeb Y (2016) Fabrication, characterization and photoelectrochemical performance of chromium-sensitized titania nanotubes as efficient photoanodes for solar water splitting. *J Solid State Electrochem* 20:683–689
  18. Momeni MM, Ghayeb Y (2015) Photoelectrochemical water splitting on chromium-doped titanium dioxide nanotube photoanodes prepared by single-step anodizing. *J Alloys Compd* 637:393–400
  19. Momeni MM, Hakimian M, Kazempour A (2015) In-situ manganese doping of TiO<sub>2</sub> nanostructures via single-step electrochemical anodizing of titanium in an electrolyte containing potassium permanganate: a good visible-light photocatalyst. *Ceram Int* 41:13692–13701
  20. Momeni MM, Ghayeb Y (2015) Fabrication, characterization and photoelectrochemical behavior of Fe–TiO<sub>2</sub> nanotubes composite photoanodes for solar water splitting. *J Electroanal Chem* 751:43–48
  21. Momeni MM, Ghayeb Y, Ghonchehi Z (2015) Fabrication and characterization of copper doped TiO<sub>2</sub> nanotube arrays by in situ electrochemical method as efficient visible-light photocatalyst. *Ceram Int* 41:8735–8741
  22. Momeni MM, Ghayeb Y (2016) Fabrication and characterization of zinc oxide-decorated titania nanoporous by electrochemical anodizing-chemical bath deposition techniques: visible light active photocatalysts with good stability. *J Iran Chem Soc* 13:481–488
  23. Momeni MM, Ghayeb Y (2015) Visible light-driven photoelectrochemical water splitting on ZnO–TiO<sub>2</sub> heterogeneous nanotube photoanodes. *J Appl Electrochem* 45:557–566
  24. Momeni MM, Ghayeb Y, Davarzadeh M (2015) Single-step electrochemical anodization for synthesis of hierarchical WO<sub>3</sub>–TiO<sub>2</sub> nanotube arrays on titanium foil as a good photoanode for water splitting with visible light. *J Electroanal Chem* 739:149–155
  25. Momeni MM, Ghayeb Y (2016) Cobalt modified tungsten–titania nanotube composite photoanodes for photoelectrochemical solar water splitting. *J Mater Sci Mater Electron* 27:3318–3327
  26. Momeni MM, Ghayeb Y (2016) Preparation of cobalt coated TiO<sub>2</sub> and WO<sub>3</sub>–TiO<sub>2</sub> nanotube films via photo-assisted deposition with enhanced photocatalytic activity under visible light illumination. *Ceram Int* 42:7014–7022
  27. Momeni MM (2015) Fabrication of copper decorated tungsten oxide–titanium oxide nanotubes by photochemical deposition technique and their photocatalytic application under visible light. *Appl Surf Sci* 357:160–166
  28. Momeni MM, Ghayeb Y (2016) Photochemical deposition of platinum on titanium dioxide–tungsten trioxide nanocomposites: an efficient photocatalyst under visible light irradiation. *J Mater Sci Mater Electron* 27:1062–1069
  29. Momeni MM, Ghayeb Y (2016) Fabrication, characterization and photocatalytic properties of Au/TiO<sub>2</sub>–WO<sub>3</sub> nanotubular composite synthesized by photo-assisted deposition and electrochemical anodizing methods. *J Mol Catal A Chem* 417:107–115
  30. Momeni MM, Nazari Z (2016) Preparation of TiO<sub>2</sub> and WO<sub>3</sub>–TiO<sub>2</sub> nanotubes decorated with PbO nanoparticles by chemical bath deposition process: a stable and efficient photocatalyst. *Ceram Int* 42:8691–8697
  31. Que L, Lan Z, Wu W, Wu J, Lin J, Huang M (2014) Titanium dioxide quantum dots: magic materials for high performance underlayers inserted into dye-sensitized solar cells. *J Power Sources* 268:670–676
  32. Choi J, Park SH, Kwon YS, Lim J, Song IY, Park T (2012) Facile fabrication of aligned doubly open-ended TiO<sub>2</sub> nanotubes, via a selective etching process, for use in front-illuminated dye sensitized solar cells. *Chem Commun* 48:8748–8750
  33. Li ZQ, Que YP, Mo LE, Chen WC, Ding Y, Ma YM, Jiang L, Hu LH, Dai SY (2015) One-pot synthesis of mesoporous TiO<sub>2</sub> microspheres and its application for high-efficiency dye-sensitized solar cells. *ACS Appl Mater Interfaces* 7:10928–10934
  34. Wu J, Hao S, Lin J, Huang M, Huang Y, Lan Z, Li P (2008) Crystal morphology of anatase titania nanocrystals used in dye-sensitized solar cells. *Cryst Growth Des* 8:247–252
  35. Lin J, Nattestad A, Yu H, Bai Y, Wang L, Doua SX, Kim JH (2014) Highly connected hierarchical textured TiO<sub>2</sub> spheres as photoanodes for dye-sensitized solar cells. *J Mater Chem A* 2:8902–8909
  36. Kushwaha R, Chauhan R, Srivastava P, Bahadur L (2015) Synthesis and characterization of nitrogen-doped TiO<sub>2</sub> samples and their application as thin film electrodes in dye-sensitized solar cells. *J Solid State Electrochem* 19:507–517
  37. Wei L, Yang Y, Fan R, Wang P, Dong Y, Zhou W, Luan T (2015) Enhance the performance of co-sensitized solar cell by a series efficient pyridine-anchor co-adsorbents of NN'-bis ((pyridin-2-yl) methylene)-p-phenylenediimine and a ruthenium dye of N719. *J Power Sources* 293:203–212
  38. Lan Z, Wu J, Lin J, Huang M (2011) A facile way to fabricate highly efficient photoelectrodes with chemical sintered scattering layers for dye-sensitized solar cells. *J Mater Chem* 21:15552–15557
  39. Hossain FM, Evteev AV, Belova IV, Nowotny J, Murch GE (2010) Electronic and optical properties of anatase TiO<sub>2</sub> nanotubes. *Comput Mater Sci* 48:854–858
  40. Berger T, Satoca DM, Jankulovska M, Villarreal TL, Gómez R (2012) The electrochemistry of nanostructured titanium dioxide electrodes. *ChemPhysChem* 13:2824–2875
  41. Choi MG, Sung YM (2014) Preparation of double layer porous films of titanium/titanium oxide for photoelectrochemical cells application. *Opt Mater* 36:1430–1435